

Uniaxial Orientational Order–Disorder Transitions in Diammine Magnesium Halides, $\text{Mg}(\text{ND}_3)_2\text{Cl}_2$ and $\text{Mg}(\text{ND}_3)_2\text{Br}_2$, Investigated by Neutron Diffraction

A. Leineweber,^{*,†,1} H. Jacobs,^{*} P. Fischer,[‡] and G. Böttger[‡]

^{*} Lehrstuhl AC I, Fachbereich Chemie der Universität, 44221 Dortmund, Germany; [†] Max-Planck-Institut für Metallforschung, Seestraße 92, 70174 Stuttgart, Germany; and [‡] Labor für Neutronenstreuung, ETHZ & PSI, 5232 Villigen PSI, Switzerland

Received September 11, 2000; accepted November 6, 2000

Neutron powder diffraction on $\text{Mg}(\text{ND}_3)_2\text{Cl}_2$ and $\text{Mg}(\text{ND}_3)_2\text{Br}_2$ revealed as a function of temperature uniaxial orientational order–disorder behavior of the ND_3 groups. The crystal structures of both compounds are built up from chains of octahedra ${}^1_{\infty}[\text{Mg}(\text{NH}_3)_2\text{X}_{4/2}]$ with $X = \text{Cl}$ and Br arranged in different ways relative to each other. At ambient temperatures ($X = \text{Cl}$) and 270 K ($X = \text{Br}$) the ND_3 groups are disordered with respect to a rotation about the bond $\text{Mg}-\text{N}$. The D atom density is well described by a fourfold split position, each D “site” connecting an N with an X atom: $\text{Mg}(\text{ND}_3)_2\text{Cl}_2$, *Cmmm*, $a = 8.1828(6)$ Å, $b = 8.2007(6)$ Å, $c = 3.7543(2)$ Å, $R(F^2)_{\text{Bragg}} = 5.9\%$; $\text{Mg}(\text{ND}_3)_2\text{Br}_2$, *Pbam*, $a = 5.9714(2)$ Å, $b = 11.9175(3)$ Å, $c = 3.98477(8)$ Å, $R(F^2)_{\text{Bragg}} = 7.9\%$. In both cases the c axis corresponds to the direction of the chains ${}^1_{\infty}[\text{Mg}(\text{NH}_3)_2\text{X}_{4/2}]$. At low temperatures (8 K ($X = \text{Cl}$) and 1.5 K ($X = \text{Br}$)) both compounds are ordered with respect to the ND_3 groups: They are arranged antiferroelectrically on either side of the chains ${}^1_{\infty}[\text{Mg}(\text{NH}_3)_2\text{X}_{4/2}]$. The symmetry is lowered compared to the situation at ambient temperatures and 270 K respectively, which involves in both cases a doubling of the orthorhombic c axis: $\text{Mg}(\text{ND}_3)_2\text{Cl}_2$, *Ibmm*, $a = 8.1319(3)$ Å, $b = 8.1338(3)$ Å, $c = 7.4410(2)$ Å, $R(F^2)_{\text{Bragg}} = 5.9\%$; $\text{Mg}(\text{ND}_3)_2\text{Br}_2$, *Pnam*, $a = 5.92837(8)$ Å, $b = 11.8448(2)$ Å, $c = 7.9117(1)$ Å, $R(F^2)_{\text{Bragg}} = 5.0\%$. Detailed evaluation of neutron diffraction data of $\text{Mg}(\text{ND}_3)_2\text{Cl}_2$ as a function of temperature ($50 \text{ K} < T < 150 \text{ K}$) characterizes the phase transition as continuous with $T_i \approx 135 \text{ K}$. © 2001

Academic Press

Key Words: diammine magnesium halides; ammoniates of magnesium halides; order–disorder transitions; dynamical disorder of ammonia ligands; neutron diffraction.

INTRODUCTION

Recently, we reported on preparation and crystal structures of the diammine magnesium halides $\text{Mg}(\text{NH}_3)_2\text{X}_2$ with $X = \text{Cl}, \text{Br}, \text{I}$ (1). These compounds crystallize in two

¹ To whom correspondence should be addressed. Fax: +49 (0)711 2095 420. E-mail: leineweber@mf.mpi-stuttgart.mpg.de.

different structure types, the $\text{Cd}(\text{NH}_3)_2\text{Cl}_2$ type (*Cmmm* (2)) for $X = \text{Cl}$ and the $\text{Mg}(\text{NH}_3)_2\text{Br}_2$ type (*Pbam* (1)) for $X = \text{Br}, \text{I}$. Both types contain parallel octahedral chains ${}^1_{\infty}[\text{Mg}(\text{NH}_3)_2\text{X}_{4/2}]$, which run along the direction $[001]$ (Fig. 1) and which are arranged in different ways relative to each other within the plane (001) (Fig. 2).

The two crystal structure types found for $\text{Mg}(\text{NH}_3)_2\text{X}_2$ with $X = \text{Cl}, \text{Br}, \text{I}$ were reported for several analogous compounds $M(\text{NH}_3)_2\text{X}_2$ ($M = \text{Mn}, \text{Fe}, \text{Co}, \text{Ni}$; $X = \text{Cl}, \text{Br}, \text{I}$) in a preliminary paper (3). More detailed investigations on $\text{Ni}(\text{NH}_3)_2\text{X}_2$ with $X = \text{Cl}, \text{Br}, \text{I}$ (4) established that for $X = \text{Br}, \text{I}$ the $\text{Mg}(\text{NH}_3)_2\text{Br}_2$ type structure is the stable modification; however, metastable phases of the $\text{Cd}(\text{NH}_3)_2\text{Cl}_2$ type structure isotypic to $\text{Ni}(\text{NH}_3)_2\text{Cl}_2$ can also be obtained.

One interesting aspect of the structures of these amines is the behavior of the NH_3 molecules with respect to a rotation about the coordinative bond $M-\text{N}$. Many studies concerning this topic are focused on hexaamines $M(\text{NH}_3)_6\text{X}_2$ with $M = \text{Ca}, \text{Mn}, \text{Fe}, \text{Co}, \text{Ni}, \text{Zn}, \text{Cd}$, and $X = \text{Cl}, \text{Br}, \text{I}$. The crystal structures of these compounds are based on a $\text{CaF}_2/\text{anti-K}_2\text{PtCl}_6$ type arrangement (5, 6). At ambient temperatures X-ray and neutron diffraction indicate disorder of the ammonia groups in such hexaamines (7–9). The dynamics of the reorientational processes were studied using various methods (10). Going to low temperatures, order–disorder phase transitions with respect to an ordering of the NH_3 groups were detected in many cases (e.g., (11)). Recently, the crystal structures of low-temperature modification of $\text{Ni}(\text{ND}_3)_6\text{X}_2$ with $X = \text{Cl}, \text{Br}, \text{I}$ were determined in which the ND_3 groups are ordered (12).

The dynamics and ordering behavior is more complicated if complex anions are involved, e.g., $X = \text{NO}_3, \text{NO}_2, \text{BF}_4$, and ClO_4 . In such compounds both order–disorder phenomena concerning a uniaxial rotation of the ND_3 groups about the bonds $M-\text{N}$ as well as a more or less free rotation of the complex anions occur. Examples for structural studies on phase transitions in such systems are, e.g., on



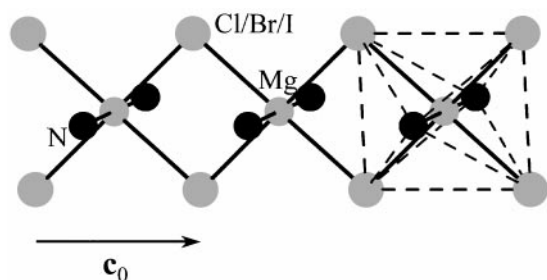


FIG. 1. Chains $\frac{1}{2}[\text{Mg}(\text{NH}_3)_2\text{X}_{4/2}]$ (with $X = \text{Cl}, \text{Br}, \text{I}; \text{H}$ omitted) of edge-sharing octahedra as main building units of $\text{Mg}(\text{NH}_3)_2\text{X}_2$ ($X = \text{Cl}, \text{Br}, \text{I}$).

$\text{Ni}(\text{ND}_3)_6(\text{NO}_3)_2$ (13), and, not belonging to the large group of K_2PtCl_6 type hexaammines, on $\text{Ag}(\text{ND}_3)_3\text{NO}_3$ (14, 15).

X-ray powder and single-crystal crystal data on $\text{Mg}(\text{NH}_3)_2\text{X}_2$ with $X = \text{Cl}, \text{Br}, \text{I}$ (1) suggest that the NH_3 groups are disordered with respect to a rotation about the bond $\text{Mg}-\text{N}$ at ambient temperatures. However, experimental evidence for the distribution of H in the $\text{Mg}(\text{NH}_3)_2\text{X}_2$ compounds is relatively weak because of the small scattering power of H for X-rays. Therefore, the results were regarded as preliminary.

Now, we report on temperature-dependent neutron diffraction data on $\text{Mg}(\text{ND}_3)_2\text{Cl}_2$ and $\text{Mg}(\text{ND}_3)_2\text{Br}_2$. In neutron diffraction the scattering power of D is within the same order of magnitude as that of the other constituting

elements. Therefore, this method is well suited to provide detailed structural data about the order-disorder phenomena with respect to ND_3 in these compounds.

EXPERIMENTAL

Preparation of $\text{Mg}(\text{ND}_3)_2\text{Cl}_2$ and $\text{Mg}(\text{ND}_3)_2\text{Br}_2$

MgCl_2 , MgBr_2 as well as their amines are sensitive toward moist air and were handled under inert gas conditions (16).

MgCl_2 (approximate batch size: 1.0 g, Alfa, 99.9%) was placed into a glass tube cooled by ice water. It was reacted with an excess of ND_3 (> 99%, Cambridge Isotope Laboratories) at ambient temperatures, yielding $\text{Mg}(\text{ND}_3)_6\text{Cl}_2$. The tube was then attached to dynamic vacuum ($p < 0.1$ Torr) and slowly heated to 120°C . This procedure removed $\frac{2}{3}$ of the ammonia from the solid leading to $\text{Mg}(\text{ND}_3)_2\text{Cl}_2$.

Anhydrous MgBr_2 was obtained by reacting Mg turnings (Ventron, > 99%) with NH_4Br (Aldrich, > 99%) in the ratio 1:2.1 in a steel autoclave (17). The product (composed of $\text{Mg}(\text{NH}_3)_2\text{Br}_2$ and NH_4Br) was placed into a glass tube attached to dynamic vacuum ($p < 0.1$ Torr). The tube was slowly heated to a maximum temperature of 350°C . The resulting product was MgBr_2 . It was characterized by X-ray diffraction and IR spectroscopy. A part of the anhydrous bromide was reacted with ND_3 to yield $\text{Mg}(\text{ND}_3)_6\text{Br}_2$, as described above for the corresponding chloride. $\text{Mg}(\text{ND}_3)_6\text{Br}_2$ and MgBr_2 were mixed in a molar ratio of

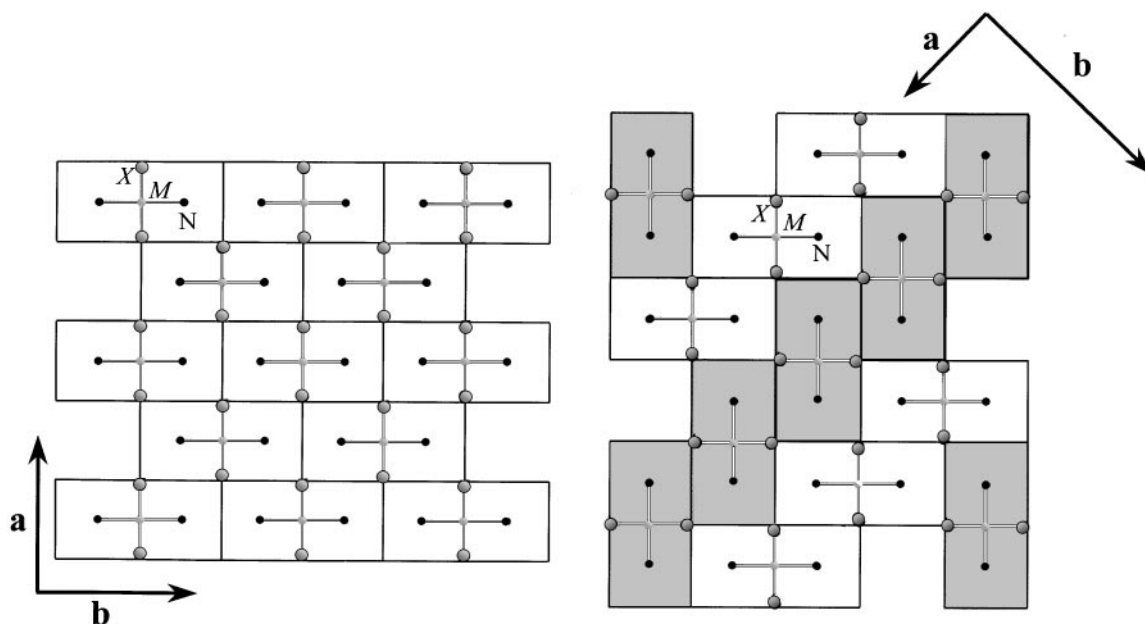


FIG. 2. Crystal structures of $\text{Mg}(\text{NH}_3)_2\text{Cl}_2$ (left) and $\text{Mg}(\text{NH}_3)_2\text{Br}_2$ (right) projected onto (001) showing the relation to a CsCl type structure: N and Cl occupy the Cs and Cl sites. Double-CsCl units are formed by connecting two CsCl units by an Mg atom on a common face. In such a double-CsCl unit an octahedron as part of a chain $\frac{1}{2}[\text{Mg}(\text{NH}_3)_2\text{X}_{4/2}]$ running along $[001]$ is located. The structures of $\text{Mg}(\text{NH}_3)_2\text{Cl}_2$ and $\text{Mg}(\text{NH}_3)_2\text{Br}_2$ (as well as $\text{Mg}(\text{NH}_3)_2\text{I}_2$) differ by the mutual arrangement of the Double-CsCl units and, therefore, of the chains $\frac{1}{2}[\text{Mg}(\text{NH}_3)_2\text{X}_{4/2}]$.

TABLE 1
Technical Data of Neutron Powder Diffraction and Rietveld Refinement of Mg(ND₃)₂Cl₂

Temperature of data collection	Ambient temperatures	8 K	50–150 K
Formula		Mg(ND ₃) ₂ Cl ₂	
Formula weight		134.32 g/mol	
Diffractometer		HRPT (SINQ, PSI, Villigen, CH)	
Wave length	1.4930 Å		1.8857 Å
2θ Range used		10°–165°	
for Rietveld refinement			
2θ Step width	0.05°		0.10°
No. of profile parameters	5	6	5
No. of background parameters	8	8	8
Space group	<i>Cmmm</i>	<i>Ibmm</i> (i.e., <i>Imma</i>)	
Lattice parameters ^a	<i>a</i> = 8.1828(6) Å <i>b</i> = 8.2007(6) Å <i>c</i> = 3.7543(2) Å	<i>a</i> = 8.1319(3) Å <i>b</i> = 8.1338(3) Å <i>c</i> = 7.4410(2) Å = 2 × 3.7205(1) Å	see Fig. 10
Cell volume, <i>Z</i>	251.93(3) Å ³ , 2	492.17(3) Å ³ , 4	
Structural parameters	14	23	
No. of independent reflections	204	350	
wR _p /R _p	0.041/0.039	0.063/0.050	
R(F ²) (F ² ≥ σ(F ²))	0.090	0.059	

^a Standard deviations do not take into account the uncertainty of the wavelength.

1:2, filled in a steel autoclave, and heated to 300°C for 3 days to yield Mg(ND₃)₂Br₂.

Care must be taken during the evacuating procedures to avoid a vigorous decomposition of the solids which may lead to a contamination of the vacuum line by the very fine powders. A glass fritted disc between sample and vacuum line may prevent this.

The final products, Mg(ND₃)₂Cl₂ and Mg(ND₃)₂Br₂, were free from impurities as to Guinier powder photographs

(CuKα₁, FR 552, Enraf Nonius, Delft (NL)), and tested by IR spectroscopy for the presence of high amounts of H.

Neutron Diffraction and Rietveld Refinement

Powdered samples were filled in vanadium cans (diameter of 8 mm) closed with gold sealings.

Neutron diffraction on Mg(ND₃)₂Cl₂ was performed on the diffractometer HRPT (18) installed at the spallation

TABLE 2
Positional and Displacement Parameters for Mg(NH₃)₂Cl₂

Atom	Wyckoff-site	<i>x</i>	<i>y</i>	<i>z</i>	<i>f</i> _{occ}	<i>U</i> _{iso} , <i>U</i> _{eq} (Å ²)
Ambient temperatures, <i>Cmmm</i>						
Mg	2 <i>a</i>	0	0	0	1	0.025(2)
Cl	4 <i>h</i>	0.2140(3)	0	$\frac{1}{2}$	1	0.0203(7)
N	4 <i>i</i>	0	0.2591(4)	0	1	0.0275(9)
D	16 <i>r</i>	0.0755(6)	0.3094(4)	0.1626(9)	$\frac{3}{4}$	0.088 ^b
8 K, <i>Ibmm</i>						
Mg	4 <i>e</i> ^a	0.0041(9)	0	$\frac{1}{4}$	1	0.006(1)
Cl	8 <i>h</i>	0.2152(2)	0	−0.0060(3)	1	0.0034(4)
N	8 <i>i</i>	0.0125(3)	0.2626(3)	$\frac{1}{4}$	1	0.0039(4)
D(a)	8 <i>i</i>	−0.0926(6)	0.3206(7)	$\frac{1}{4}$	1	0.032 ^b
D(b)	16 <i>j</i>	0.0746(4)	0.3079(4)	0.3562(3)	1	0.026 ^b

^a These Wyckoff site labels refer to the standard setting *Imma*. The origin for the high temperature phase is (00 $\frac{1}{4}$) with respect to the coordinates of the low-temperature phase.

^b The coefficients of the *U*_{ij} tensor are given in Table 5. $U_{eq} = \frac{1}{3} \text{Tr}(U_{ij})$.

TABLE 3
Technical Data of Neutron Powder Diffraction and Rietveld Refinement of Mg(ND₃)Br₂

Temperature of data collection:	270 K	1.5 K
Formula	Mg(ND ₃) ₂ Br ₂	
Formula weight	224.24 g/mol	
Diffractometer	D1A (ILL, Grenoble (F))	
Wavelength	1.9114 Å	
2θ Range	10°–155°	
2θ Step width	0.05°	
No. of profile parameters	6	6
No. of background parameters	4	5
Space group	<i>Pbam</i>	<i>Pnam</i> (i.e., <i>Pnma</i>)
Lattice parameters ^a	<i>a</i> = 5.9714(2) Å <i>b</i> = 11.9175(3) Å <i>c</i> = 3.98477(8) Å	<i>a</i> = 5.92837(8) Å <i>b</i> = 11.8448(2) Å <i>c</i> = 7.9117(1) Å = 2 × 3.95586(7) Å
Cell volume, <i>Z</i>	283.57(1) Å ³ , 2	555.56(2) Å ³ , 4
Structural parameters	25	43
No. of independent reflections	194	349
w <i>R</i> _p / <i>R</i> _p	0.051/0.039	0.048/0.037
<i>R</i> (<i>F</i> ²) (<i>F</i> ² ≥ σ(<i>F</i> ²))	0.079	0.050

^aStandard deviations do not take into account the uncertainty of the wavelength.

neutron source SINQ at the PSI (Villigen (CH)). Low temperatures were achieved by a closed-cycle helium cryostat.

For the detailed structure analyses performed at 8 K and ambient temperatures diffraction data were collected with $\lambda = 1.4930$ Å and a stepwidth of 0.05° in order to have

a wide range of *d* spacings. Whereas at ambient temperatures the high-intensity mode was used, higher resolution was obtained for $T = 8$ K by primary collimation $\alpha_1 = 12'$ and secondary collimation $\alpha_2 \approx 24'$. Faster data acquisition was desired for the characterization of the phase transition in the range $8 \text{ K} \leq T \leq 150 \text{ K}$. Here, $\lambda = 1.8857$ Å and a stepwidth of 0.1° was used. The data were corrected for absorption by measuring the transmission of the sample at $\lambda = 1.8857$ Å. From this the absorption for 1.4930 Å was calculated.

Neutron diffraction on Mg(ND₃)₂Br₂ was performed on the diffractometer D1A (19) installed at the ILL (Grenoble (F)) with a wavelength of 1.9114 Å. Low temperatures were generated by a standard Orange Cryostat. For these data no absorption correction was applied.

Rietveld refinement was performed using the GSAS package of programs (20). Neutron scattering lengths used were 0.6674 fm for D, 0.930 fm for N, 0.5375 fm for Mg, 0.9579 fm for Cl, and 0.679 fm for Br. The background of the diffraction patterns was fitted using shifted Chebichev polynoms. The reflection profiles were fitted by an exponential Pseudo-Voigt convolution as implemented in the GSAS package.

RESULTS AND DISCUSSION

Evaluation of Neutron Diffraction Data Taken at Ambient Temperature

Neutron diffraction data of Mg(ND₃)₂Cl₂ taken at ambient temperatures as well as of Mg(ND₃)₂Br₂ taken at 270 K show only reflections which can totally be indexed with the unit cell parameters obtained from the X-ray diffraction

TABLE 4
Positional and Displacement Parameters for Mg(NH₃)₂Br₂

Atom	Wyckoff site	<i>x</i>	<i>y</i>	<i>z</i>	<i>f</i> _{occ}	<i>U</i> _{iso} , <i>U</i> _{eq} (Å ²)
270 K, <i>Pbam</i>						
Mg	2 <i>a</i>	0	0	0	1	0.013(1)
Br	4 <i>h</i>	0.2776(6)	0.3858(4)	$\frac{1}{2}$	1	0.0133(9)
N	4 <i>g</i>	0.2497(7)	0.1250(4)	0	1	0.0230(9)
D	8 <i>i</i>	0.365(1)	0.1120(5)	0.146(2)	$\frac{3}{4}$	0.073 ^b
D'	8 <i>i</i>	0.228(1)	0.1875(6)	0.154(2)	$\frac{3}{4}$	0.100 ^b
1.5 K, <i>Pnam</i>						
Mg	4 <i>c</i> ^a	0.002(1)	0.0006(6)	$\frac{1}{4}$	1	0.003(1)
Br	8 <i>d</i>	0.2788(4)	0.3872(2)	0.0005(4)	1	−0.0039(5)
N(1)	4 <i>c</i>	0.2575(6)	0.1224(4)	$\frac{1}{4}$	1	−0.0004(8)
D(1a)	4 <i>c</i>	0.213(1)	0.2014(7)	$\frac{1}{4}$	1	0.050 ^b
D(1b)	4 <i>d</i>	0.3616(8)	0.1163(5)	0.1541(6)	1	0.038 ^b
N(2)	4 <i>c</i>	0.7476(7)	0.8735(4)	$\frac{1}{4}$	1	0.0045(8)
D(2a)	4 <i>c</i>	0.593(1)	0.8954(8)	$\frac{1}{4}$	1	0.061 ^b
D(2b)	8 <i>d</i>	0.758(1)	0.8190(4)	0.1553(6)	1	0.041 ^b

^aThese Wyckoff site labels refer to the standard setting *Pnma*. The origin for the high-temperature phase is (00 $\frac{1}{4}$) with respect to the coordinates of the low-temperature phase.

^bThe coefficients of the *U*_{ij} tensor are given in Table 5. $U_{eq} = \frac{1}{3} \text{Tr}(U_{ij})$.

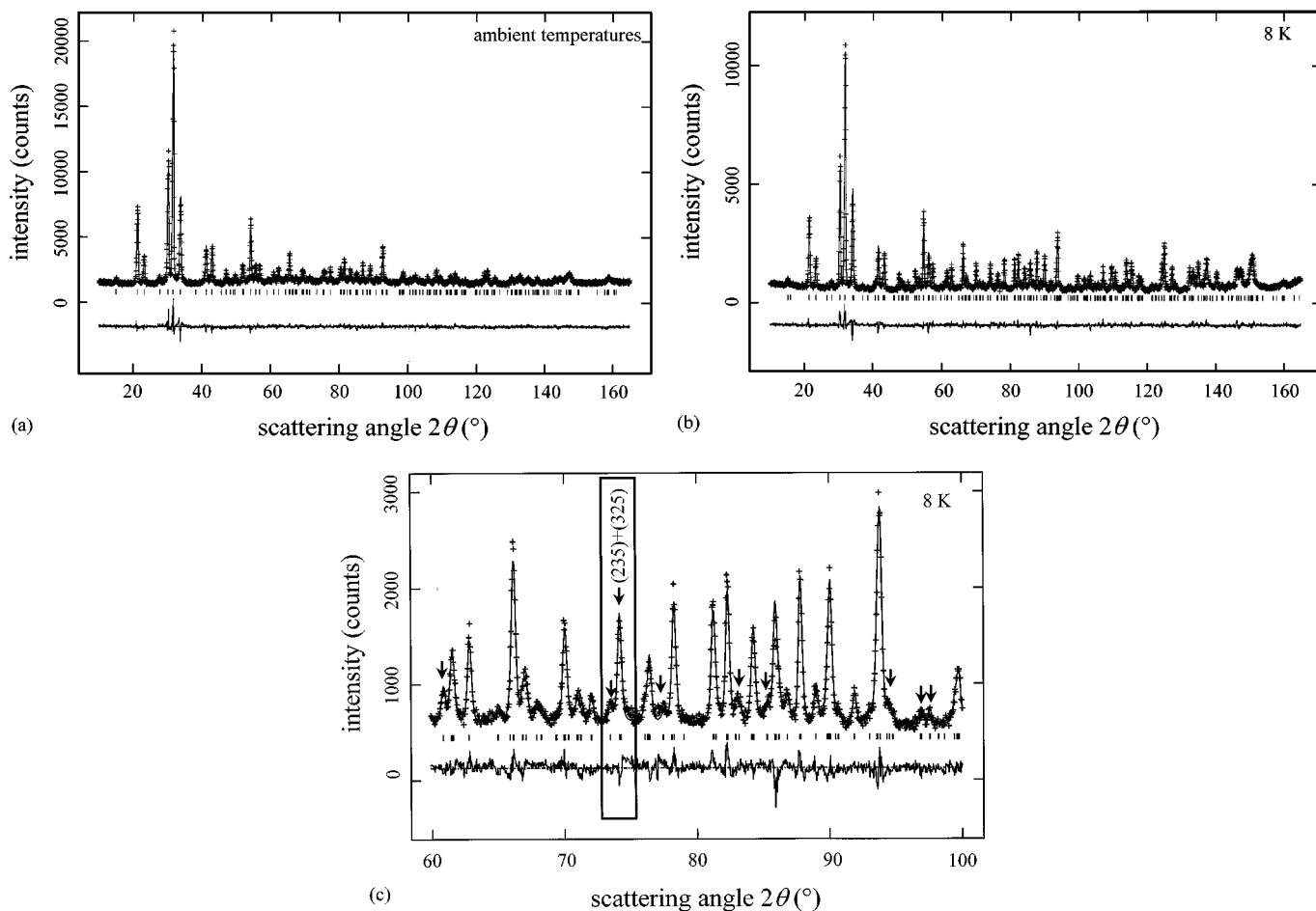


FIG. 3. Observed (+) and calculated (–) neutron diffraction profiles (top) and difference curve (bottom) of $\text{Mg}(\text{NH}_3)_2\text{Cl}_2$ ($\lambda = 1.4930 \text{ \AA}$): ambient temperatures (a) and 8 K (b). Markers indicate positions of reflections of the high- and low-temperature phase, respectively. (c) An enlarged part of (b) depicting some superstructure reflections and showing in a box the part of the patterns with the strong pair of superstructure reflections (235) + (325) used to analyze the temperature-dependent evolution of the superstructure using $\lambda = 1.8857 \text{ \AA}$ data.

data (1). Rietveld refinements were performed using structural models with a disordered distribution of three D atoms over four sites, as used for the evaluation of the experimental data of Ref. (1). All positional parameters, isotropic thermal parameters for Mg, Cl/Br, and N as well as anisotropic thermal parameters for the D sites were refined successfully. Technical data of the measurements and the refinements are summarized in Tables 1 and 3, the structural parameters are given in Tables 2 and 4.

Figures 3a and 4a show the diffraction patterns including Rietveld fits. Figures 5a and 5b give the octahedra $\text{Mg}(\text{ND}_3)_2\text{Cl}_4$ and $\text{Mg}(\text{ND}_3)_2\text{Br}_4$ as building units of the chains $\frac{1}{\infty}[\text{Mg}(\text{ND}_3)_2X_{4/2}]$ (Figs. 6a and 6b). For $\text{Mg}(\text{ND}_3)_2\text{Cl}_2$ we additionally illustrate the distribution of D by Fourier sections (F_{obs}) through the plane formed by the D atoms (Fig. 7).

The distribution of D in $\text{Mg}(\text{ND}_3)_2\text{Cl}_2$ and $\text{Mg}(\text{ND}_3)_2\text{Br}_2$ is similar to that obtained by detailed single-crystal neutron

diffraction studies on $\text{Ni}(\text{ND}_3)_6\text{Br}_2$ at ambient temperatures (9). That compound belongs to the $\text{CaF}_2/\text{anti-K}_2\text{PtCl}_6$ structure type (space group $Fm\bar{3}m$) with Ca replaced by the octahedral complex cation. The ND_3 molecules point with their D atoms toward a square of Br atoms. The site symmetry of N (C_{4v}) is incompatible with the threefold symmetry of the ND_3 molecules (C_{3v}). This incompatibility is overcome by a rotation of the ND_3 molecules about the axis Ni–N. The rotation is accompanied by a translational motion of the ND_3 molecules, i.e. the N atoms are slightly displaced from the fourfold axis (21). Time-averaging finally yields the observed distribution of D with four maxima of density pointing toward the Br atoms.

The local environment of ND_3 by X in $\text{Mg}(\text{ND}_3)_2\text{Cl}_2$ and $\text{Mg}(\text{ND}_3)_2\text{Br}_2$ is similar to that in $\text{Ni}(\text{ND}_3)_6\text{Br}_2$. The positively charged part of the ND_3 dipole is directed toward a rectangle of X anions which is close to a square (Figs. 5a and 5b). The site symmetry of N is C_{2v} and C_s for

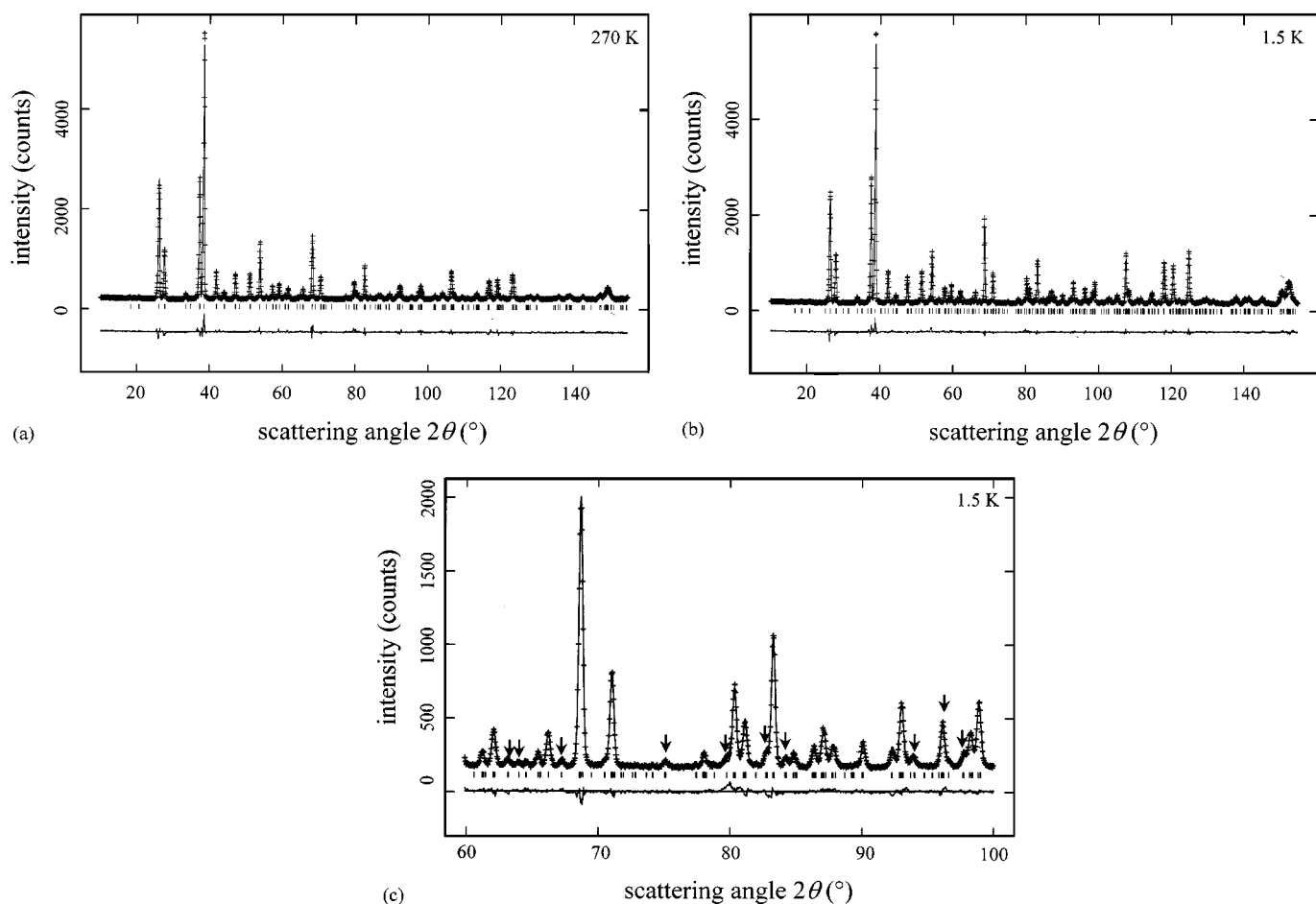


FIG. 4. Observed (+) and calculated (−) neutron diffraction profiles (top) and difference curve (bottom) of $\text{Mg}(\text{NH}_3)_2\text{Br}_2$ ($\lambda = 1.9114 \text{ \AA}$): 270 K (a) and 1.5 K (b). Markers indicate positions of reflections of the high- and low-temperature phase, respectively. (c) An enlarged part of (b) depicting some superstructure reflections.

$\text{Mg}(\text{ND}_3)_2\text{Cl}_2$ and $\text{Mg}(\text{ND}_3)_2\text{Br}_2$, respectively. C_{2v} is again incompatible with C_{3v} ; however, C_S is compatible. Actually, for $\text{Mg}(\text{ND}_3)_2\text{Br}_2$ ordering is possible without a reduction of symmetry. Nevertheless, the distribution of D is disordered as in $\text{Mg}(\text{ND}_3)_2\text{Cl}_2$. The decisive reasons for disorder at ambient temperatures are interatomic potentials and entropy. In fact, it is shown in the next section that the most simple type of ordering of ND_3 in $\text{Mg}(\text{ND}_3)_2\text{Br}_2$, which would preserve the $Pbam$ symmetry, is not formed at low temperatures.

Evaluation of Neutron Diffraction Data at Low Temperatures

The diffraction patterns of $\text{Mg}(\text{ND}_3)_2\text{Cl}_2$ and of $\text{Mg}(\text{ND}_3)_2\text{Br}_2$ taken at 8 and 1.5 K, respectively, show additional reflections, compared to the situation at 295 and 270 K, respectively, (Figs. 3 and 4). In both cases, the superstructure reflections can be attributed to a doubling of the

c axes of either unit cell. However, structure solution is not straightforward because many of the superstructure reflections are quite weak. Furthermore, an unambiguous indexing of the new reflections is not possible as both crystal structure types under consideration have pseudotetragonal cell dimensions ($a \approx b$ and $2a \approx b$, respectively; compare Tables 1 and 3, discussed in detail in Ref. (1)). Therefore, we constructed different ordered starting models to be tested by Rietveld refinement.

As discussed previously for the hexaammines (9, 21, 22), the particular orientation of the ammonia groups should mainly depend on interactions $\text{H} \cdots \text{X}$ (ammonia group with neighboring anions) and $\text{H} \cdots \text{H}$ (between different ammonia groups). As in the hexaammines one has to expect frustration for the interactions $\text{H} \cdots \text{X}$ as these cannot fully be optimized due to the incompatibility of the threefold symmetry of the ammonia group and the approximate fourfold symmetry of the environment of the ammonia group by X (see Fig. 5). The interactions $\text{H} \cdots \text{H}$ are expected to be

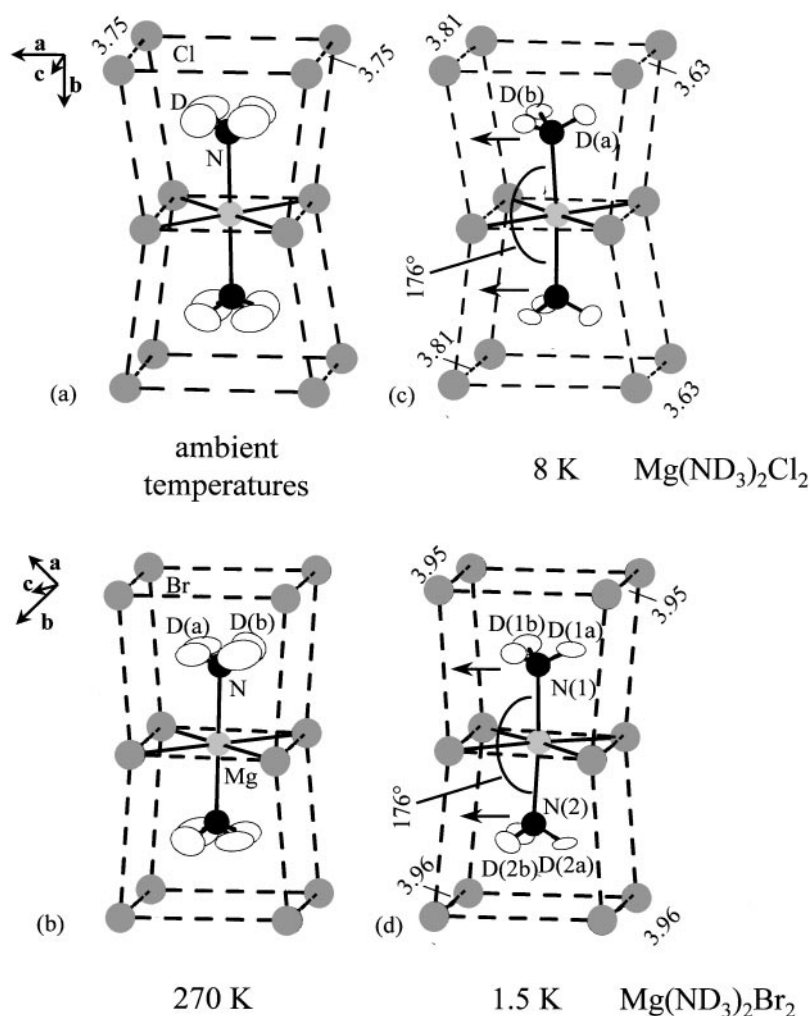


FIG. 5. Units $\text{Mg}(\text{ND}_3)_2\text{Cl}_4$ (a and c) and $\text{Mg}(\text{ND}_3)_2\text{Br}_4$ (b and d) as constituents of the chains $\frac{1}{\infty}[\text{Mg}(\text{ND}_3)_2\text{X}_{4/2}]$ with ND_3 molecules pointing toward rectangles of X. Only for the D atoms information about displacement parameters is given (50% probability).

repulsive. In $\text{Mg}(\text{ND}_3)_2\text{Cl}_2$ and $\text{Mg}(\text{ND}_3)_2\text{Br}_2$ they should be strongest between ammonia groups which are adjacent on one side of an octahedral chain. Here, the distance $\text{N} \cdots \text{N}$ (which carry the interacting D atoms) is closest and corresponds the length of the cell parameter of the disordered phase, c_0 . As the superstructure formation involves a doubling of c_0 it is suggested that the ND_3 molecules order in the way shown in Fig. 8. Such an “antiferroelectric” left–right–left ordering of the D(a) atoms on the mirror planes \cdots/m should be favored in terms of electrostatic interactions. In contrast, a “ferroelectric” right–right–right (identical to left–left–left) ordering which retains the translation c_0 , should be avoided. An arrangement like this could be constructed for $\text{Mg}(\text{ND}_3)_2\text{Br}_2$ in its original unit cell with $Pbam$ symmetry as mentioned in the section above.

Favoring a doubling of c_0 and the ordering principle as to Fig. 8 and assuming, furthermore, that all octahedral chains

are equivalent, four different superstructures can be constructed for each of the two structure types under consideration. This number arises from two possibilities how to arrange two ND_3 groups bonded to one Mg, which we call *eclipsed* and *staggered* (analogous to the conformations of ethane molecules) and, additionally, from two possibilities of orientation for the chains with the Mg atoms at $(\frac{1}{2} \frac{1}{2} z)$ compared to those at $(00z)$.

Figures 9 and 10 show schematically the four different superstructures derived for $\text{Mg}(\text{ND}_3)_2\text{Cl}_2$ and of $\text{Mg}(\text{ND}_3)_2\text{Br}_2$, respectively. The space groups of the superstructures are subgroups of the order 2, resulting from doubling of c_0 of the space groups $Cmmm$ and $Pbam$ of the high-temperature phase, respectively (23). Note that the mirror planes \cdots/m are preserved in all structural models.

Testing these structure models in Rietveld refinement yields convincing fits in $Ibmm$ ($Imma$) for $\text{Mg}(\text{ND}_3)_2\text{Cl}_2$ and

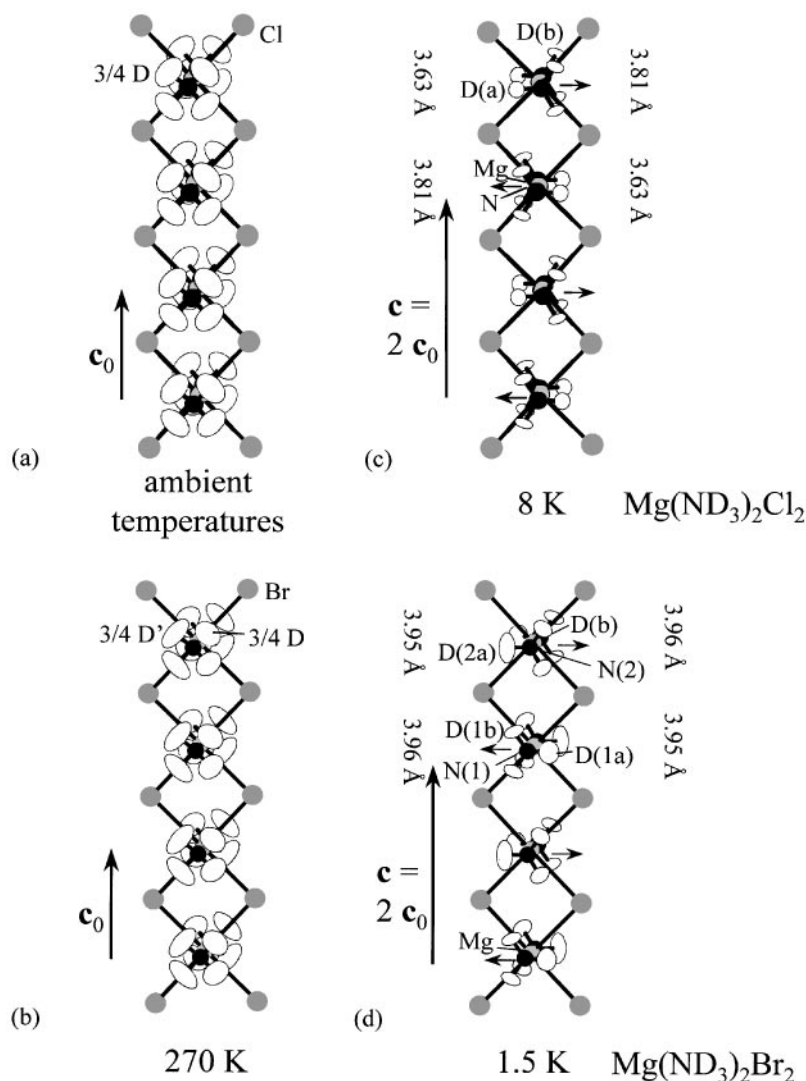


FIG. 6. Chains of octahedra $\frac{1}{2}[\text{Mg}(\text{ND}_3)_2X_{4/2}]$ present in $\text{Mg}(\text{ND}_3)_2\text{Cl}_2$ (a and c) and $\text{Mg}(\text{ND}_3)_2\text{Br}_2$ (b and d). For the c and d (low-temperature phases) the arrows indicate the displacements of the ND_3 molecules. Only for the D atoms information about displacement parameters is given (50% probability).

in $Pnam$ ($Pnma$) for $\text{Mg}(\text{ND}_3)_2\text{Br}_2$. The low-temperature phase structure model of the chloride leads to two different kinds of D sites, labeled D(a), situated on the mirror planes \dots/m , and D(b) (Fig. 8). For $\text{Mg}(\text{ND}_3)_2\text{Br}_2$ the “left” and “right” orientation of the ND_3 molecules are inequivalent in symmetry because of the specific mutual arrangement of the chains $\frac{1}{2}[\text{Mg}(\text{ND}_3)_2X_{4/2}]$. Therefore, one yields four D sites (D(1a), D(1b), D(2a), D(2b)) and consequently two N sites (N(1) and N(2)).

Details and results of Rietveld refinements are given in Tables 1–5, bond lengths and angles are listed in Table 6. Figures 5c and 5d show the octahedra $\text{Mg}(\text{ND}_3)_2X_4$ displaying thermal ellipsoids for D. A Fourier section (F_{obs}) through the D atoms of an ND_3 molecule of the low-temperature phase of $\text{Mg}(\text{ND}_3)_2\text{Cl}_2$ is plotted in Fig. 7.

The D(b) atoms are directed approximately to X atoms, which obviously involves hydrogen bonding, whereas the D(a) atoms point between two X atoms (Figs. 5c and 5d). The nuclear scattering density of D is significantly more smeared out than that of the Mg, X, and N atoms. This is exhibited by the thermal parameters (Tables 2 and 4). It cannot be said from these data whether this is due to thermal motion of D in a very soft potential or due to a superposition of two or more minima of energy of a single ND_3 molecule in its local environment. For the chloride the form of the ellipsoids is compatible with mainly librational motion of the D atoms. For the bromide the refinement of U_{ij} components of the D atoms leads to a significant improvement of residuals. However, details of the U_{ij} tensors as well as the values of the other thermal parameters

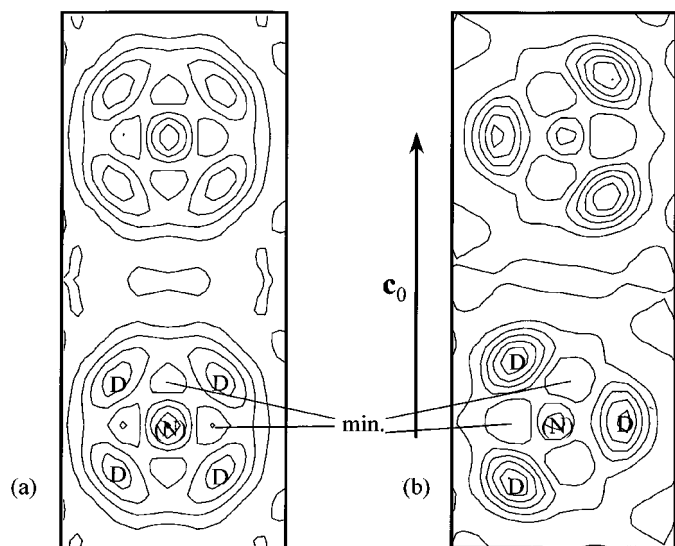


FIG. 7. Fourier sections (F_{obs}) for $\text{Mg}(\text{ND}_3)_2\text{Cl}_2$ for ambient temperatures (a) and 8 K (b) data. Each time six equidistant steps of nuclear scattering density were chosen between 0 and the maximum density. For (a) the section shows the a plane (010) at a height $y = 0.3094$, for (b) at $y = 0.3143$.

should be treated with care due to the high minimum d spacings of diffraction data compared to those measured for the chloride.

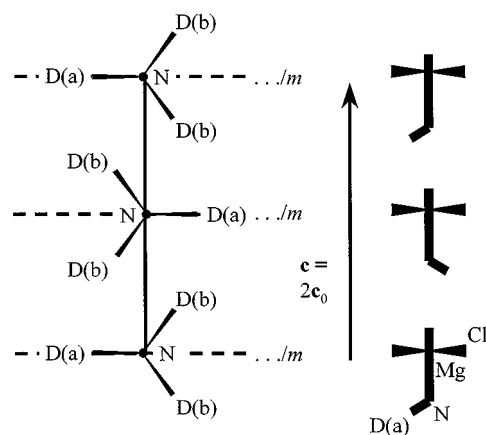


FIG. 8. "Antiferroelectric" model for ordering of ND_3 groups on one single side of a chain $\frac{1}{\infty}[\text{Mg}(\text{ND}_3)_2\text{X}_{4/2}]$ in the LT phase of $\text{Mg}(\text{ND}_3)_2\text{Cl}_2$ and $\text{Mg}(\text{ND}_3)_2\text{Br}_2$. It can be regarded to be energetically favored in terms of repulsive interactions $\text{D} \cdots \text{D}$ and implies a doubling of the c axis. On the left one looks on a chain viewed along the axes $\text{N}-\text{Mg}-\text{N}$. Cl is not shown. The ND_3 groups are oriented in such a way that one sort of D (called D(a)) lies on mirror planes \cdots/m . These are used to represent the ordering on the right. The three pictograms show the Mg, N, and D(a) atoms on the three single-mirror planes \cdots/m with additional Cl atoms above and below the mirror planes (view along $[001]$). For the "antiferroelectric" ordering scheme, the orientation of the ND_3 groups in one single-mirror plane is sufficient to represent the ordering of the whole structure.

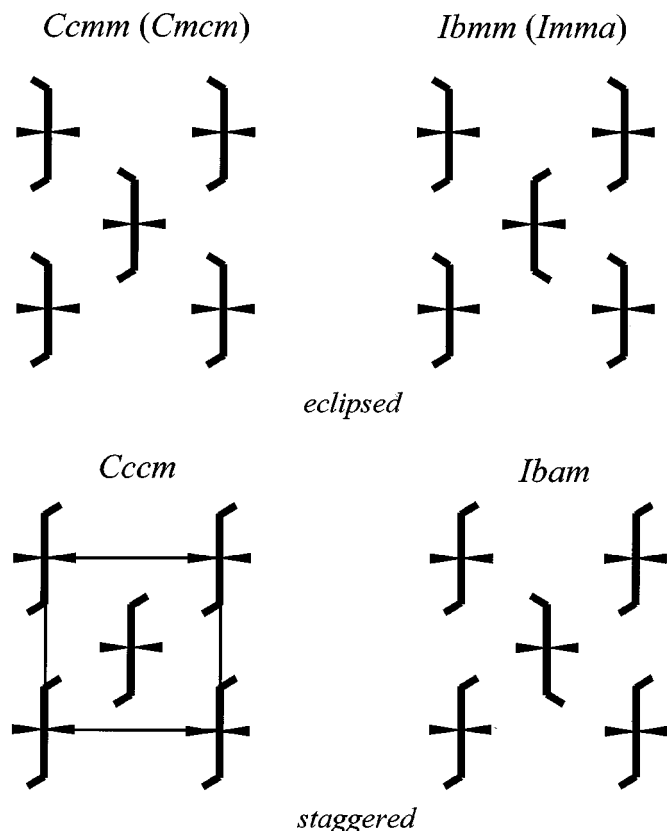


FIG. 9. Schematic illustration of possible ordering types of $\text{Mg}(\text{ND}_3)_2\text{Cl}_2$ with an "antiferroelectric" arrangement of the ND_3 molecules and one type of chain, $\frac{1}{\infty}[\text{Mg}(\text{ND}_3)_2\text{Cl}_{4/2}]$. Compare Fig. 8 for the meaning of the pictograms. Within an unit cell there is a second plane (001) with all D(a) on the other side of N.

The ordering of the ND_3 molecules leads to additional atomic displacements relative to the positions in the high temperature phases. The most prominent feature of both low temperature phases is a bending of the angles $\text{N}-\text{Mg}-\text{N}$ from 180° to 176° which accompanies the eclipsed conformation of the $\text{D}_3\text{N}-\text{Mg}-\text{ND}_3$ units (Figs. 5c and 5d). The bending leads to a displacement of N of about 0.07 \AA from its mean position of the disordered phase and further reduces the repulsive electrostatic interactions of adjacent ND_3 molecules of one ordered side of chain $\frac{1}{\infty}[\text{Mg}(\text{ND}_3)_2\text{X}_{4/2}]$ along $[001]$. Furthermore, these displacements move the D(b) atoms of the ND_3 molecules toward pairs of X atoms. Thereby, the hydrogen bonds $\text{N}-\text{D(b)} \cdots \text{X}$ become more efficient.

The displacements of the N atoms in the low-temperature phase of the diammines are of similar magnitude as the displacements in the disordered phases of hexaammines (21) derived from an analysis of the coupling of rotational and translational motion of ammonia. One might imagine that similar displacements may also be present in the high-

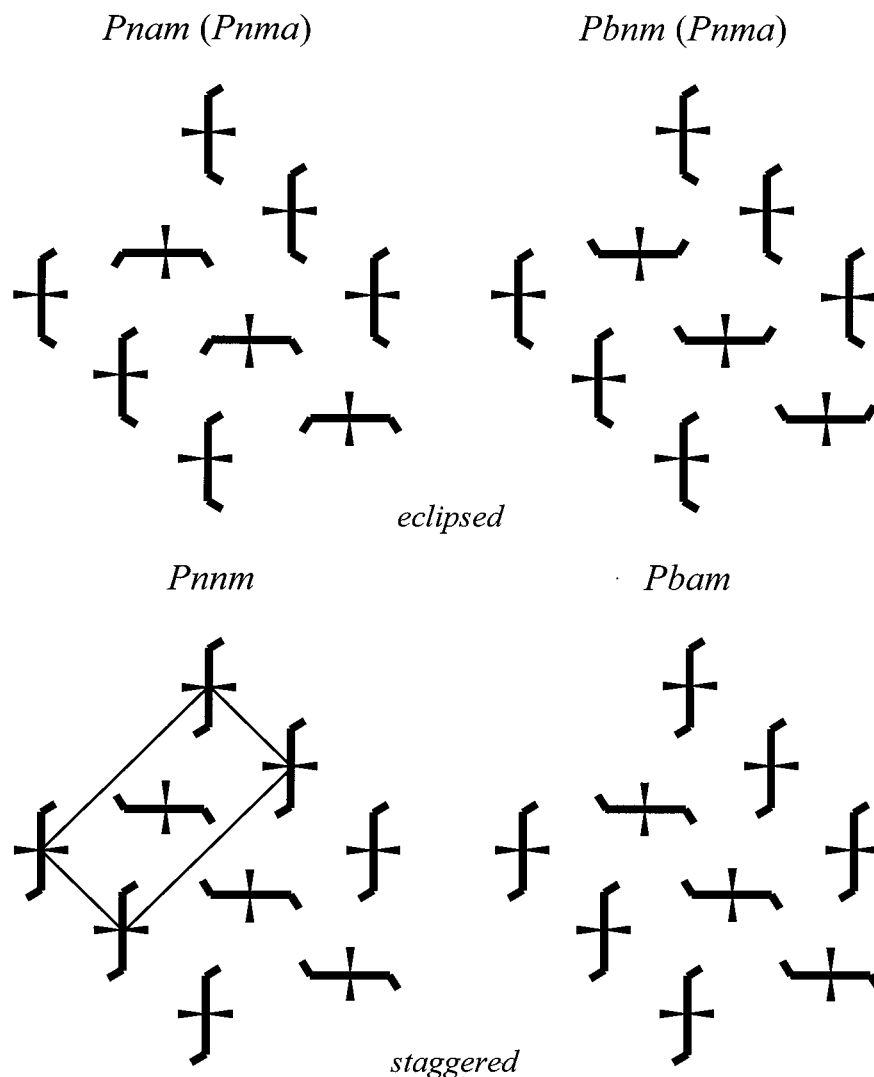


FIG. 10. Schematic illustration of possible ordering types of $\text{Mg}(\text{ND}_3)_2\text{Br}_2$ in a way as done in Fig. 9 for $\text{Mg}(\text{ND}_3)_2\text{Cl}_2$.

temperature phases of the diammines. Evidence for this comes from the fact that the U_{iso} values for N in the high-temperature phases are larger than those of Mg and X (see Tables 2 and 4).

Furthermore, in the low-temperature phase of the chloride the Cl atoms are displaced from the planes (001) at $z = 0$ and 0.5 which are mirror planes in the high-temperature phase at $z = 0.5$ (compare Table 2). This yields short (3.63 Å) and long (3.81 Å) distances Cl ... Cl along [001]. The short distance results when two D(a) atoms from different ND_3 molecules (only one of these ND_3 molecules is shown in Fig. 5c) point to a pair Cl ... Cl, the long ones when 2×2 D(b) are involved. The consequences for the geometry of a single chain are illustrated in Fig. 6c. For the bromide the displacements of Br along [001] are much

smaller (Figs. 5d and 6d). This is attributed to the fact, that, in contrast to the situation in the chloride, one D(a) and two D(b) atoms point to each pair Br ... Br.

Given the "antiferroelectric" arrangement of ND_3 molecules on one side of the chains $\frac{1}{\infty}[\text{Mg}(\text{ND}_3)_2\text{X}_{4/2}]$, it is difficult to discuss the reasons why the particular observed low-temperature phase structures are formed out of the four models constructed for the chloride and the bromide, respectively (Figs. 9 and 10). Most probably there is no general rule behind the fact that in both cases an eclipsed conformation of the $\text{D}_3\text{N-Mg-ND}_3$ units is present. Strikingly, in the low-temperature modifications of $\text{Ni}(\text{ND}_3)_6\text{X}_2$ with $\text{X} = \text{Cl, Br, I}$ (12) which all exhibit different ordering patterns of ND_3 , always an eclipsed conformation is present. However, in a medium temperature modification of

TABLE 5
Components of the U_{ij} Tensors^a of the D-sites in $\text{Mg}(\text{ND}_3)_2\text{Cl}_2$ and $\text{Mg}(\text{ND}_3)_2\text{Br}_2$

Atom		U_{11} (\AA^2)	U_{22} (\AA^2)	U_{33} (\AA^2)	U_{12} (\AA^2)	U_{13} (\AA^2)	U_{23} (\AA^2)
$\text{Mg}(\text{ND}_3)_2\text{Cl}_2$	295 K						
D		0.098(5)	0.060(3)	0.107(3)	-0.007(2)	-0.042(3)	-0.026(2)
$\text{Mg}(\text{ND}_3)_2\text{Cl}_2$	8 K						
D(a)		0.032(3)	0.028(3)	0.037(3)	0.007(2)	0	0
D(b)		0.041(2)	0.019(2)	0.017(1)	-0.002(1)	-0.010(1)	-0.008(1)
$\text{Mg}(\text{NH}_3)_2\text{Br}_2$	270 K						
D(1)		0.055(4)	0.071(4)	0.093(5)	-0.030(3)	-0.028(3)	0.007(4)
D(2)		0.083(5)	0.089(5)	0.128(7)	-0.023(7)	0.042(5)	-0.060(5)
$\text{Mg}(\text{NH}_3)_2\text{Br}_2$	1.5 K						
D(1a)		0.038(5)	0.034(4)	0.078(7)	-0.021(4)	0	0
D(1b)		0.039(3)	0.047(3)	0.027(3)	-0.012(3)	0.010(2)	-0.013(3)
D(2a)		0.019(4)	0.027(4)	0.14(1)	-0.015(3)	0	0
D(2b)		0.051(3)	0.030(2)	0.041(3)	-0.009(3)	0.011(3)	-0.007(3)

^aThe anisotropic thermal displacement factor exponent takes the form $-2\pi^2 [h^2 a^{*2} U_{11} + \dots + 2hka^*b^* U_{12}]$.

$\text{Ni}(\text{ND}_3)_6(\text{NO}_3)_2$ (13) the staggered conformation is observed. The crystal structure of the low-temperature phases of this compound are unknown.

Temperature Dependence of Ordering in $\text{Mg}(\text{ND}_3)_2\text{Cl}_2$

In order to characterize the order-disorder transition in $\text{Mg}(\text{ND}_3)_2\text{Cl}_2$ neutron diffraction data were recorded between 50 and 150 K with $\lambda = 1.8857 \text{ \AA}$. As expected, the superstructure reflections become weaker with increasing temperatures, finally disappearing between 130 and 140 K, as shown in Fig. 11.

Comparing the distributions of D atoms observed at 8 and 295 K and the models used for their description reveals that the D density must be redistributed in a relatively complicated way. Furthermore, taking into account the lower range of d spacings available with the wavelength of 1.8857 \AA compared to the measurements at 8 and 295 K taken with 1.4930 \AA neutrons we did not try to evaluate the D densities in detail. Instead, we restricted our analysis on an evaluation of superstructure reflection intensities. This was performed on the overlapping (due to pseudotetragonal cell dimensions) pair of strong superstructure reflections (235) and (325). In order to determine the sum of their intensities as a function of temperature the angular range of $93.5^\circ < 2\theta < 99.5^\circ$ was chosen to be fitted. This is shown for the 1.4930 \AA data in Fig. 3c. The reflections additional to (235) + (325) in this range can be assigned to an additional pair or superstructure reflections (451) + (541) of lower intensity than (235) + (325) as well as to a weak reflection which must be assigned to be originated by an impurity. The latter is also present above the phase transition temperature. In this range there is additionally a fundamental reflection (006) ((003) with respect to the HT phase) with negligible

intensity. The fit was performed using three ($T \leq 110 \text{ K}$) and two Gaussian peaks ($T \geq 120$) assigned to (451) + (541), (235) + (325), impurity and (235) + (325) and impurity, respectively. The sum of reflection intensities (235) + (325) is plotted as a function of temperature in Fig. 11, confirming a continuous decay of reflection intensities up to the phase transition at about 135 K. Attempts to fit the temperature dependence of the reflection intensities according to a critical behavior suffer from the apparent deviation from a simple behavior observed around 100 K. Therefore, no details are given.

The continuous order-disorder phase transition $Ibmm \rightarrow Cmmm$ is compatible with Landau theory as the order of space groups changes by a factor of two (24). For

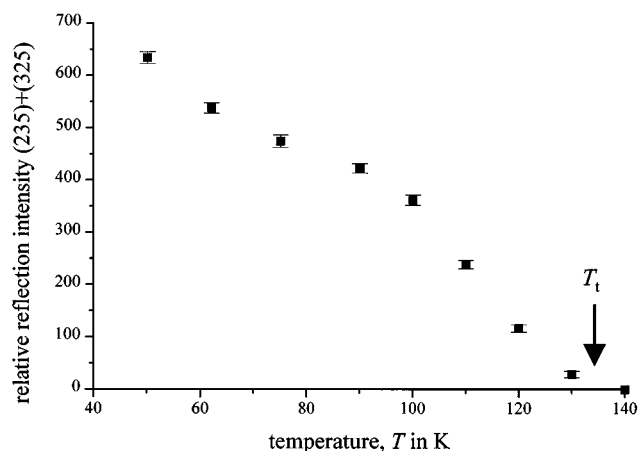


FIG. 11. Sum of intensities of the reflections (235) and (325) as a function of temperature illustrating the continuous phase transition $Ibmm \rightarrow Cmmm$ in $\text{Mg}(\text{ND}_3)_2\text{Cl}_2$. The intensities were obtained by peak fitting using a Gaussian peak shape.

TABLE 6
Distances and Angles in Mg(ND₃)₂Cl₂ and Mg(ND₃)₂Br₂

	Mg(NH ₃) ₂ Cl ₂	295 K	Mg(NH ₃) ₂ Cl ₂	8 K	Mg(NH ₃) ₂ Br ₂	270 K	Mg(NH ₃) ₂ Br ₂	1.5 K
Distances (Å)								
Mg-	4 × X	2.567(2)	2 × X	2.564(5)	4 × X	2.754(2)	2 × X	2.723(5)
			2 × X	2.545(5)			2 × X	2.724(5)
	2 × N	2.125(3)	2 × N	2.137(2)	2 × N	2.108(3)	1 × N(1)	2.092(8)
							1 × N(2)	2.132(8)
N/N(1)-	4 × D	0.961(5)	1 × D(a)	0.976(5)	2 × D	0.915(6)	1 × D(1a)	0.972(8)
			2 × D(b)	1.008(3)	2 × D'	0.974(7)	2 × D(1b)	0.981(5)
N(2)-							1 × D(2a)	0.951(7)
							2 × D(2b)	0.990(5)
D-	1 × D ... Cl		2 × D(a) ... Cl		1 × D ... Br		2 × D(1a) ... Br	
		2.649(4)		2.805(2)		2.839(6)		2.982(6)
			1 × D(b) ... Cl		1 × D' ... Br		1 × D(1b) ... Br	
				2.570(4)		2.752(8)	2 × D(2a) ... Br	2.756(5)
							1 × D(2b) ... Br	2.966(6)
								2.745(5)
Angles (°)								
D-N-D	2 × 79.9(4) ^a		2 × 105.2(3)		1 × 79(1) ^a		N(1):	
	2 × 78.9(4) ^a		1 × 103.4(4)		1 × 78(1) ^a		1 × 101.3(6)	
	2 × 129.2(7) ^a				2 × 80.3(4) ^a		2 × 104.1(6)	
					2 × 129.6(6) ^a		N(2):	
							1 × 98.4(6)	
							2 × 103.7	
Mg-N-D	4 × 115.4(3)		1 × 117.0(4)		2 × 114.4(5)		N(1):	
			2 × 112.5(3)		2 × 116.4(6)		1 × 117.8(6)	
							2 × 113.8(5)	
							N(2):	
							1 × 119.2(7)	
							2 × 114.6(4)	
N-D ... X	D:		D(a):		D:		D(1a):	
	1 × 167.1(3)		2 × 137.7(2)		1 × 165.4(6)		2 × 132(1)	
			D(b):		D':		D(1b):	
			1 × 153.6(2)		1 × 163.3(3)		1 × 155(1)	
							D(2a):	
							2 × 135(1)	
							D(2b):	
							1 × 156(2)	
N-Mg-N	180		176.3(4)		180		176(1)	
Bridging	86.0(2)		86.50(6)		87.3(1)		86.84(6)	
X-Mg-X								

^a These angles are not bonding angles but result from the description of the mean distribution within the disordered structure by split sites of D.

Mg(ND₃)₂Br₂ the phase transition *Pnam* → *Pbam* is expected to occur in a similar fashion. Probably, the transition temperature of the bromide is lower than that of the chloride, which is also observed for many hexaammines (11).

Cell parameters for Mg(ND₃)₂Cl₂ as a function of temperature were determined by Rietveld refinement. Structural models used for data at *T* ≤ 100 K were those of the low-temperature phase, at higher temperatures, for simplicity, those of the high-temperature phase. Thermal and posi-

tional parameters will not be discussed for reasons mentioned above. Lattice parameters and unit cell volumes, normalized to the values obtained at 8 K, are plotted in Fig. 12. The unit cell volume shows no anomaly at the phase transition temperature. Furthermore, the cell parameters show no discontinuity at that point. A continuous phase transition demands this. However, the anisotropy of thermal expansion changes at the phase transition. Below the temperature of the phase transition, *c* increases strongly compared to the other axes. This is explained by increasing

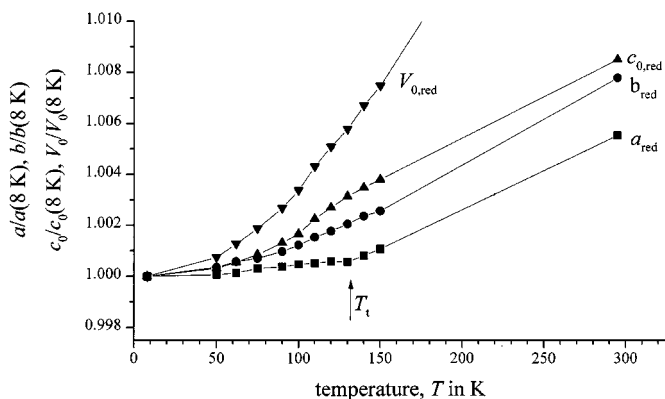


FIG. 12. Cell parameters and unit cell volumes for $\text{Mg}(\text{ND}_3)_2\text{Cl}_2$, normalized to the values at 8 K. V_0 and c_0 refer to the translation vector of the high-temperature phase, which is doubled in the low-temperature phase. The arrow indicates the phase transition temperature.

repulsive interactions between ND_3 groups with increasing disorder along the chains.

CONCLUSION

For $\text{Mg}(\text{ND}_3)_2\text{Cl}_2$ and $\text{Mg}(\text{ND}_3)_2\text{Br}_2$ uniaxial orientational order-disorder phase transitions were characterized by means of neutron diffraction. In the low-temperature modifications the D atoms are ordered in contrast to the situation in the high-temperature phase stable at ambient temperatures.

An interesting comparison is that between amines and hydrates. $\text{Mg}(\text{H}_2\text{O})_2\text{Cl}_2$ (25) is isotypic to the corresponding Mn, Fe, and Co compounds (26, 27) and contains octahedral chains $\frac{1}{\infty}[\text{Mg}(\text{H}_2\text{O})_2X_{4/2}]$, which are arranged relative to each other as in $\text{Mg}(\text{NH}_3)_2\text{Cl}_2$. The symmetry is, however, monoclinic, $C2/m$, caused by uniaxial rotational ordering of the H_2O molecules which is present at ambient temperatures. The H_2O molecules can adapt well to the local environment of X atoms. Both H atoms point directly to an X atom. Therefore, no frustration of the interactions $\text{H} \cdots X$ occurs, in contrast to the amines. Hydrates crystallizing similarly to the $\text{Mg}(\text{NH}_3)_2\text{Br}_2$ type structure are not known. $\text{Mn}(\text{H}_2\text{O})_2\text{Br}_2$ and $\text{Fe}(\text{H}_2\text{O})_2\text{Br}_2$ are isotypic to the corresponding chlorides (28).

The observed changes of the long-range order in the amines presented in this paper which results from the evaluation of elastic neutron diffraction considering Bragg reflections are most probably accompanied by changes of the rotational dynamics of the ND_3 groups. However, spectroscopic methods are needed to get a deeper insight in the dynamics in these compounds.

ACKNOWLEDGMENTS

DIA measurements were performed during CRG-funded beam time. A.L. acknowledges financial support during the HRPT measurement by the Laboratory for Neutron Scattering of ETHZ and PSI. Furthermore, financial support by the "Bundesministerium für Bildung, Wissenschaft, Forschung und Technologie" (JA5DOR) and the "Fonds der Chemischen Industrie" is gratefully acknowledged. We thank Petra Schiebel (Institut für Kristallographie, Universität Tübingen) for discussion.

REFERENCES

1. A. Leineweber, M. W. Friedriszik, and H. Jacobs, *J. Solid State Chem.* **147**, 229 (1999).
2. C. H. MacGillavry and J. M. Bijvoet, *Z. Kristallogr.* **94**, 249 (1936).
3. A. Leineweber, M. W. Friedriszik, H. Jacobs, R. Essmann, G. Böttger, F. Fauth, and P. Fischer, *Z. Kristallogr. Suppl.* **16**, 46 (1999).
4. A. Leineweber and H. Jacobs, *J. Solids State Chem.* **152**, 381 (2000).
5. R. W. G. Wyckoff, "Crystal Structures," Vol. 3, p. 783. Interscience, New York, 1965.
6. I. Olvson, *Acta Crystallogr.* **18**, 889 (1965).
7. H. Jacobs, J. Bock, and C. Stüve, *J. Less-Common Met.* **134**, 207 (1987).
8. R. Eßmann, G. Kreiner, A. Niemann, D. Rechenbach, A. Schmieding, T. Sichla, U. Zachwieja, and H. Jacobs, *Z. Anorg. Allg. Chem.* **622**, 1161 (1996).
9. A. Hoser, W. Prandl, P. Schiebel, and G. Heger, *Z. Phys. B Condensed Matter* **81**, 259 (1990).
10. J. M. Janik, J. A. Janik, A. Migdał-Mikuli, E. Mikuli, and K. Otnes, *Physica B* **168**, 45 (1991).
11. L. Asch, G. K. Senoy, J. M. Friedt, J. P. Adloff, and R. Kleinberger, *J. Chem. Phys.* **62**, 2335 (1975).
12. P. Schiebel, Institut für Kristallographie, Universität Tübingen, *private communication*.
13. A. F. Andresen, H. Fjellvåg, J. A. Janik, J. Mayer, J. Ściensinki, J. M. Janik, A. Migdał-Mikuli, E. Mikuli, M. Rachwalaska, and T. Stanek, *Physica B* **138**, 295 (1986).
14. U. Zachwieja, Ph.D. thesis, Universität Dortmund, 1991.
15. H. Jacobs, R. Niewa, T. Sichla, A. Tenten, and U. Zachwieja, *J. Alloys Compd.* **246**, 91 (1997).
16. H. Jacobs and D. Schmidt, *Curr. Top. Mater. Sci.* **8**, 379 (1982).
17. B. Nöcker, Ph.D. thesis, Universität Dortmund, 1991.
18. P. Fischer, G. Frey, M. Koch, M. Könnecke, V. Pomjakushin, J. Schefer, R. Thut, N. Schlumpf, R. Bürge, U. Greuter, S. Bondt, and E. Berruyer, *Physica B* **276–278**, 146 (2000).
19. A. W. Hewat and I. Bailey, *Nucl. Instrum. Methods* **137**, 463 (1976).
20. A. C. Larson and R. B. von Dreele, General Structure Determination System (GSAS). Los Alamos National Laboratory, Los Alamos, NM, 1995.
21. P. Schiebel, A. Hoser, W. Prandl, G. Heger, W. Paulus, and P. Schweiss, *J. Phys. Condens. Matter* **6**, 10989 (1994).
22. A. R. Bates and K. W. H. Stevens, *J. Phys. C* **2**, 1573 (1969).
23. Th. Hahn, "International Tables for Crystallography," Vol. A. Kluwer Academic Publishers, Dordrecht, 1995.
24. J. C. Tolédano and P. Tolédano, "The Landau Theory of Phase Transitions." World Scientific, Singapore, 1987.
25. A. Leineweber, R. Niewa, and H. Jacobs, *unpublished*.
26. B. Morosin and E. J. Graeber, *Acta Crystallogr.* **16**, 1176 (1963).
27. B. Morosin and E. J. Graeber, *J. Chem. Phys.* **42**, 898 (1965).
28. B. Morosin, *J. Chem. Phys.* **47**, 417 (1967).